Effects of working parameters on the performance of cyclone separator for rapeseed combine harvester based on CFD

Xingyu Wan[1], Jiacheng Yuan[1], Jia Yang[1], Yitao Liao[1,2], Qingxi Liao[1,2*]

(1. *College of Engineering, Huazhong Agricultural University, Wuhan 430070, China*;
2. *Key Laboratory of Agricultural Equipment in Mid-lower Reaches of the Yangtze River, Ministry of Agriculture and Rural Affairs, Wuhan 430070, China*)

Abstract: Existing development for cyclone separation cleaning components of the rapeseed combine harvester, which employs the suspending airflow to separate the rapeseeds from the materials other than grain (MOG), has the challenge to figure out the optimal working parameters, highlighting a need for exploration of the invisible airflow based on Computational Fluid Dynamics (CFD). The airflow status was mainly affected by the air velocities of the inlet, and the outlet for the MOG. The single factor and response surface experiments were carried out. It could be found that the inlet and MOG outlet velocities affected the air velocities through the change in the air quantity. Furthermore, the mathematical model of the relationship between the air velocities inside the cyclone and the working parameters was built, and the optimal combination of working parameters was obtained by multi-objective optimization. The inlet and outlet velocities of the optimal combination were 4.25 m/s and 29.87 m/s, respectively. Under this condition, the cleaning ratio and loss ratio of the cleaning device was 94.62% and 5.39%, respectively, as validated by the field experiment. The findings provide references for the improvement of cleaning systems for rapeseed combine harvesters.

Keywords: rapeseed, combine harvester, cyclone separation cleaning, optimal working parameters, CFD
DOI: 10.25165/j.ijabe.20231601.7253

Citation: Wan X Y, Yuan J C, Yang J, Liao Y T, Liao Q X. Effects of working parameters on the performance of cyclone separator for rapeseed combine harvester based on CFD. Int J Agric & Biol Eng, 2023; 16(1): 128–135.

1 Introduction

As a widely used method for rapeseed harvesting, combine harvesting can realize cutting, threshing, separation, and cleaning functions[1,2], leading to relatively higher production efficiency and less labor consumption compared with the windrower[3,4]. One of the issues for combine harvesting is the proper period for harvesting is short. It requires high adaptability for rapeseed plants. However, most of the rapeseed combine harvesters are modified based on the wheat or rice combine harvesters to increase the operation rate of the vehicle. Adding a vertical cutting device on one side of the header, extending the depth of the header, changing the type of sieves, and adjusting related parameters are the conventional modifying measures[5,6]. Modified combine harvesters have the problems of high loss and low cleaning ratio of the seeds. It means that special combine harvesters for rapeseed harvesting are in demand. The cleaning device, which directly affects the cleaning ratio and loss ratio, plays an important role[7]. The fan and vibration sieve are utilized in combine harvesters which may have the problems of large size and high vibration. Therefore, a new kind of cleaning device with a simple structure and good performance should be considered to solve those problems.

With the development of cyclone separators in the factorial field, the cyclone separation cleaning device becomes one of the research directions of cleaning equipment for combine harvesters. Cyclone separation cleaning devices based on the airflow cleaning method is used for the grain combine harvester in recent years due to their relatively simple structure[8-10]. Liao et al.[11] designed a kind of cyclone separation cleaning system whose main working components were cyclone separator, forced feeding conveyor, pipe, and fan. Wan et al.[12,13] added a cylinder sieve or a conical sieve to help reduce the load of the cyclone separator. Jin et al.[14] did some researches on the physical movement analysis to solve the problems of halfway separating and the high loss rate of the cyclone separation system by using high-speed photography. The cyclone separator is the crucial part. The materials will be separated under the function of the suspending airflow and different centrifugal forces[15-17].

One of the challenges is how to figure out the invisible gas phase in the cyclone separator. Computational Fluid Dynamic (CFD), Particle Image Velocimetry (PIV), etc. were the approaches that could be utilized to achieve the goal. The CFD method is widely applied in industry and agriculture fields. Elsayed et al.[18] optimized a new set of geometrical ratios to achieve minimum pressure drop based on CFD. Hamed et al.[19] carried out the numerical study of the fluid flow and particle dynamics by CFD to characterize the performance of new design cyclone separators with one, two, and three tangential inlets. Huang et al.[20] built the finite element models of cyclone separation sand samplers with different sizes to find out the optimal structure based on CFD.

Receive date: 2021-12-08 **Accepted date:** 2022-11-13
Biographies: Xingyu Wan, PhD, research interest: modern agricultural equipment design, measurement and control, Email: wanxy@mail.hzau.edu.cn; **Jiacheng Yuan**, PhD candidate, research interest: modern agricultural equipment design, measurement and control, Email: 2944112901@qq.com; **Jia Yang**, MS candidate, research interest: modern agricultural equipment design, measurement and control, Email: 1850939908@qq.com; **Yitao Liao**, PhD, Professor, research interest: modern agricultural equipment design, measurement and control, Email: liaoetao@mail.hzau.edu.cn.
***Corresponding author: Qingxi Liao**, PhD, Professor, research interest: modern agricultural equipment design, measurement and control. College of Engineering, Huazhong Agricultural University, Wuhan 430070, China. Tel: +86-27-87282121, Email: liaoqx@mail.hzau.edu.cn.

Zhao et al.[21] carried out the optimization analysis of two different models of cyclone separator with or without the bucket, and the mathematical relationship model was established between bucket length, diameter and escape time, loss rate, and pressure drop. According to those researchers, the structural and working parameters of the cyclone separator have a great influence on the performance of the cyclone separator.

In a word, the CFD approach could be an effective way to find out the effects of the working parameters on the performance of cyclone separators for the rapeseed combine harvester. This work introduced the process of the cyclone separator for the rapeseed combine harvester and applied the CFD model to obtain the airflow status inside the cyclone separator with different inlet and MOG outlet velocities. The airflow was divided into the high-velocity area and the low-velocity area based on the air velocity distribution to discuss the performance of the cyclone separator. The influence of each parameter was studied, and a better combination of the working parameters was put forward. It could provide a reference for improving the optimization of cleaning device for rapeseed combine harvesters.

2 Materials and methods

2.1 Main structure and working process of the combine harvester

Figure 1 showed the structure of the 4LYZ-2.0 type of rapeseed combine harvester. It mainly consisted of the header, shredding device, longitudinal axial flow threshing and separating device, and cyclone separation cleaning device. The power for the devices except for the walking system was provided by the hydraulic system to realize the quick and independent adjustment of the working parameters. In the field, the cutting device in the header cut off the rapeseed plants with the help of the reel. The rapeseed plants were sent into the shredding device which would be cut into pieces and transferred to the longitudinal axial flow threshing and separating device. The cyclone separation cleaning device took the responsibility to separate the rapeseeds in the threshing outputs generated in the threshing and separating device. The threshing outputs were the mixtures of rapeseeds, pod shells, short stems, and light MOG.

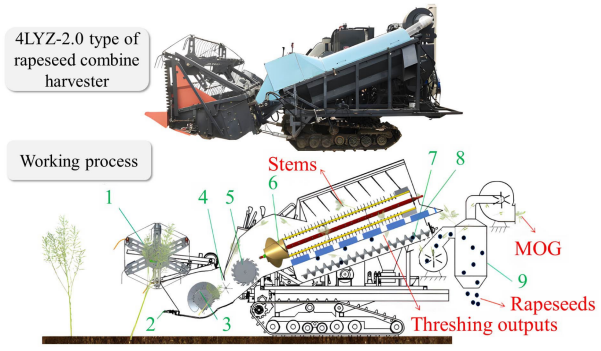

1. Reel 2. Cutting device 3. Spiral conveyor 4. Feeding roller 5. Shredding device 6. Threshing cylinder 7. Threshing outputs conveyor 8. Sieve 9. Cyclone separation cleaning device.

Figure 1 Structure of the 4LYZ-2.0 type rapeseed combine harvester

Figure 2 shows the working process of the cleaning device. The cyclone separation cleaning system mainly consisted of the blower, cyclone separator, fan, and pipe. The inlet of the fan and the outlet of the cyclone separator for the MOG were connected by the pipe. The blower could provide an initial velocity for the threshing outputs when it entered the cyclone separator. Furthermore, the rotating of the blower impeller could affect the air velocity of the cyclone separator inlet. At the same time, the suspending airflow was generated when the fan worked. In a word, the main working parameters of the cyclone separator were the velocities of inlet and outlet for the MOG. The MOG were siphoned off through the pipe and centrifugal fan to the field. The rapeseeds fell and were collected. The cyclone separator could divide into three parts which were the upper cone part, the lower cone part, and the cylinder part. In terms of the airflow field inside the cyclone separator, there existed an area concentrated along the center axis with a higher air velocity. It could be called the high-velocity area. The other space beyond the high-velocity area could be called the low-velocity area. The working parameters of the cyclone were the inlet and MOG outlet velocities.

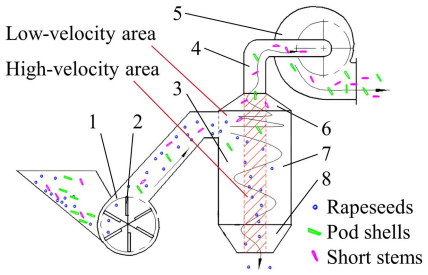

1. Blower 2. Impeller 3. Cyclone separator 4. Pipe 5. Fan 6. Upper cone 7. Cylinder part 8. Lower cone.

Figure 2 Working process of the cyclone separation cleaning device

2.2 Computational Conditions and Parameters

The CFD technique was used to solve the equations based on the software of Fluent (ANSYS). The 3D model of the designed cyclone separator, as the basis of numerical simulation, affected the results of the simulation. Figure 3 shows the schematics of the computational grid and structural parameters of the cyclone separator. Two velocity inlets (one for the materials inlet, the other for the MOG outlet) and pressure outlet were applied for the inlet and outlets of the airflow in all the simulations. The motion of the gas phase was solved with the Standard k-ε turbulence model. Walls were assumed to the material of steel, and their positions were fixed. The CFD time step was defined as 4×10^{-3} s for a total simulation time of 1.0 s.

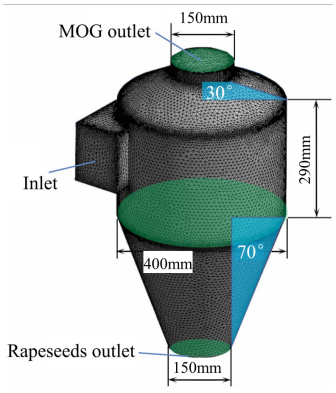

Figure 3 Schematics of computational grids

2.3 Simulation Method

To find out the effects of inlet and outlet velocities, the single factor and the response surface experiments were carried out. The indexes to figure out the performance of the cyclone separator could be the average air velocity, velocity distribution of high-velocity area and low-velocity area, and the velocity and pressure along the center axial direction. Figure 4 shows the location of the planes in the simulation. The difference between

the velocities of the high-velocity and the low-velocity areas could be utilized to represent the performance of the high-velocity area. The larger the difference meant the air was more concentrated in the high-velocity area. At the same time, the average air velocities of horizontal planes should be close to ensure the stability of the airflow in the cylinder part. To ensure the performance of the cyclone, the air velocities in the low-velocity area and high-velocity area of plane 1 should be larger than 1.2 m/s and 6.3 m/s which matched the suspending air velocity of the light MOG and short stems, respectively[11]. The single-factor experiment could find out the change rules between the single working parameter and the indexes. In the experiment of the inlet air velocity, the range of the inlet air velocity was 1-5 m/s whilst the MOG outlet air velocity was 25 m/s. The inlet air velocity kept to be 5 m/s while the range of the MOG outlet air velocity was 20-30 m/s. And, the response surface experiment would be carried out under these ranges to obtain the optimal combination of the working parameters.

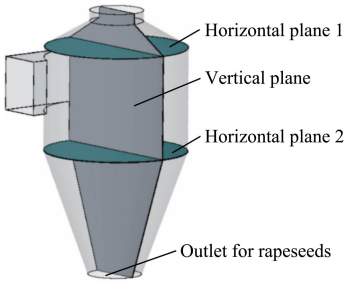

Figure 4 Planes built for obtaining the data

2.4 Validation of the simulation model and optimal parameters

To validate the accuracy of the optimal working parameters, bench tests and field experiments were carried out. The bench test relied on the multi-function test platform for rape combine harvester (Figure 5), which was mainly composed of a feeding conveyor belt, header, threshing separation device, cyclone separation cleaning device, etc. All operating components were driven by motors and had adjustable rates. The inlet and MOG outlet velocities of the cyclone separator could be measured by an air velocity tester (ZC1000-1F, Shanghai Yiou Instrument Equipment Co., Ltd., China). The accuracy of the simulation model was validated by the relative error obtained by comparing the simulated value and actual value of the air velocity at the center of the rapeseed outlet[22].

Before the test, rapeseed plants were evenly spread on the feeding conveyor belt, and the rate of the thrower and fan were adjusted to make the inlet and MOG outlet velocities reach the optimal parameter combination. The corresponding thrower and fan rates were recorded. After that, the conveyor belt, header, and other components were started to complete the combined harvesting process. The experiment would repeat 3 times, and the materials that came from the rapeseed outlet of cyclone separator and fan outlet were collected. After that, the rapeseed and MOG would be separated and weighed to calculate the cleaning ratio and loss ratio of the rapeseed as below:

$$Y_q = \frac{m_1}{m_0} \times 100\% \quad (1)$$

$$Y_s = \frac{m_2}{m_1 + m_2} \times 100\% \quad (2)$$

where, Y_q and Y_s are the cleaning ratio and loss ratio of the cyclone separation cleaning device, respectively; m_0 is the mass of all the materials that came from the rapeseed outlet of cyclone separator, kg; m_1 is the mass of rapeseed that came from the rapeseed outlet of cyclone separator, kg; m_2 is the mass of rapeseed came from the fan outlet, kg.

1. Feeding conveyor belt 2. Header 3. Threshing and separation device 4. Cycone separation cleaning device 5. Fan 6. Pipe 7. Cyclone separator 8. Blower

Figure 5 Multi-functional test platform for rapeseed combine harvester

To validate whether the cyclone separator could work well or not under the field conditions, the field experiments of 4LYZ-2.0 type rapeseed combine harvester were carried out at the modern agricultural science and technology base of Huazhong Agricultural University. The variety of rapeseed was Huayouza 62, planted by the direct seeder. The experimental area was 5000 m^2. The planting density and moisture content of rape-seed plants would be tested before the experiments. The structure and operation parameters of each device were under the optimal parameter combination. The inlet and MOG outlet velocities of the cyclone separator would be adjusted with the help of the air velocity tester. The harvester would go ahead 10 m at the speed of 0.8 m/s by 3 times. The calculation method of the cleaning ratio and loss ratio was the same as that used in the bench test.

3 Results and discussion

3.1 Effects of inlet air velocity on airflow status

Figure 6 showed the effects of the inlet air velocity. In plane 1 and plane 2, it was indicated that the velocities in the high-velocity area were higher than that in the low-velocity area, which proved the existence of the areas. With the increase of the inlet air velocity, the average velocity decreased as well as the velocities in both high-velocity and low-velocity areas. The relationship between the inlet air velocity and the air velocity of the outlet for the MOG was linear. The total air quantity was invariable when the outlet air velocity was not changed. The airflow went into the cyclone separator through the inlet and the outlet for the rapeseeds. The air quantity from the outlet for the MOG decreased when the inlet air velocity increased, leading to a decrease in the average air velocity in plane 1. At the same time, the axial air velocity in plane 1 was relatively stable. Both the axial velocities of the high-velocity and the low-velocity area were higher than any of the others when the inlet air velocity was 1.5 m/s. It meant the air velocity was more concentrated in the axial direction. In plane 2, the average air velocity decreased when the inlet air velocity increased. However, the average and axial air velocities of the high-velocity area started increasing when the inlet air velocity increased from 3 m/s. It reflected that the air velocity was concentrated in the high-velocity area. In terms of the axial air velocity distribution along the center axial, the velocities in the cylinder part were lower due to its larger diameter. The air velocity in the cylinder part increased, and the air velocity in the lower cone decreased when the inlet air velocity increased.

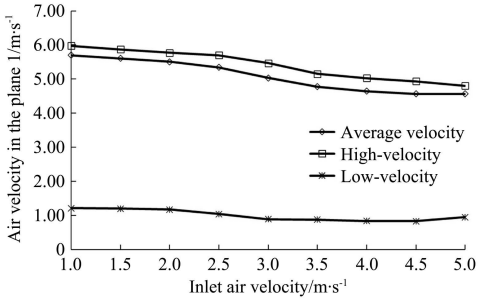

a. Effects of the inlet air velocity on the air velocities in the horizontal plane 1

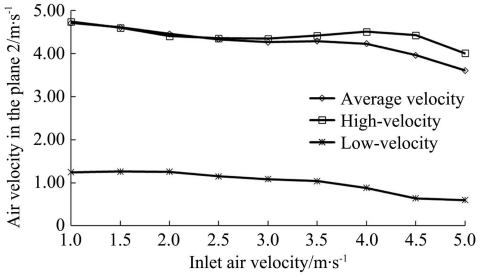

b. Effects of the inlet air velocity on the air velocities in the horizontal plane 2

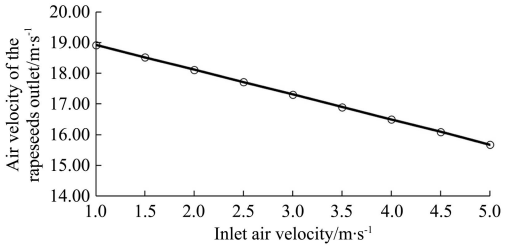

c. Effects of the inlet air velocity on the air velocities in the rapeseeds outlet

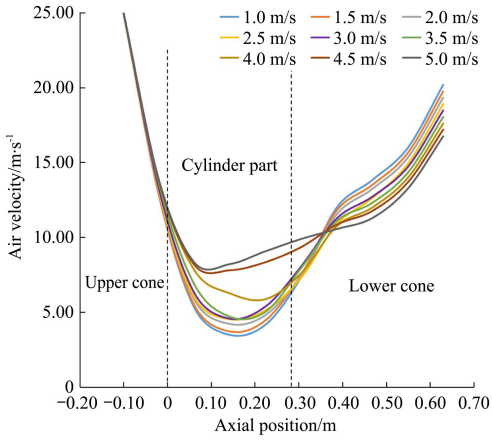

d. Effects of the inlet air velocity on the air velocities along the center axis

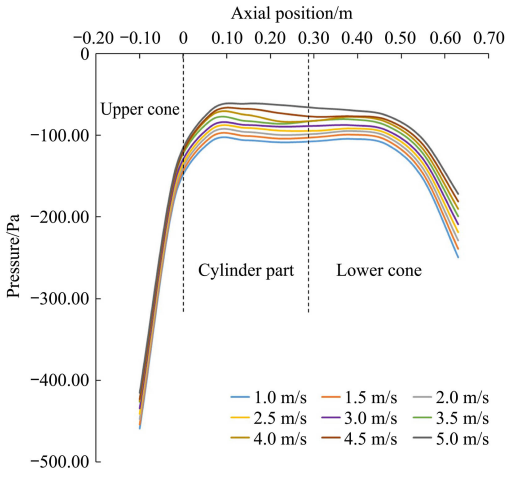

e. Effects of the inlet air velocity on the negative pressure along the center axis

Figure 6 Effects of the inlet air velocity on the airflow status

The values of the air velocity in the cylinder part obviously increased when the inlet air velocity was in the range of 4-5 m/s. The reason was that the total air quantity was constant when the air velocity and sectional area of the MOG outlet do not change, namely, the total air quantity was equal to the sum of the air quantity of inlet and air quantity of the rapeseed outlet. With the increase of inlet air velocity, the air quantity of inlet would increase, leading to reducing of air that came through the lower cone. In terms of the axial pressure distribution along the center axial, the negative pressure was higher when the inlet air velocity was lower.

3.2 Effects of MOG outlet air velocity on airflow status

Figure 7 shows the effects of the outlet air velocity. The simulated value of the air velocity at the center of the rapeseed outlet was 17.83 m/s when the inlet and MOG outlet air velocity were set as 5 m/s and 28 m/s, respectively. And the actual value was 18.06 m/s which means the relative error was calculated to be 1.27%. It indicated that the simulation model was reasonable and could be used to analyze the airflow field distribution inside the cyclone separator.

All the velocities increased with the increase of the outlet air velocity. More air quantity was needed when the outlet air velocity increased if the inlet air velocity did not change. The linear relationship between the air velocity of the outlet for the rapeseeds and the outlet air velocity was a result. In plane 1, the average air velocity and the air velocity of the high-velocity area increased faster than the others. It meant outlet air velocity had an

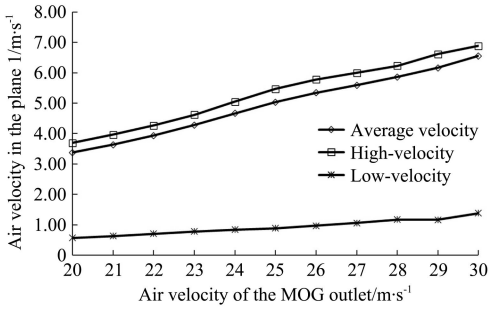

a. Effects of the MOG outlet air velocity on the air velocities in the horizontal plane 1

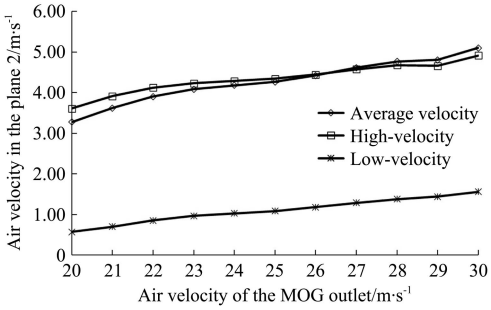

b. Effects of the MOG outlet air velocity on the air velocities in the horizontal plane 2

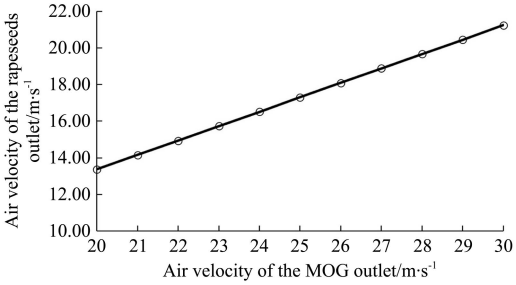

c. Effects of the MOG outlet air velocity on the air velocities in the rapeseeds outlet

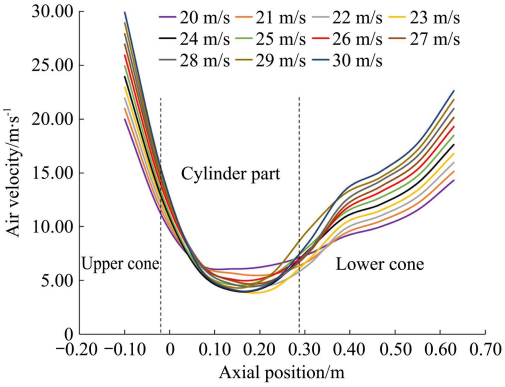

d. Effects of the MOG outlet air velocity on the air velocities along the center axis

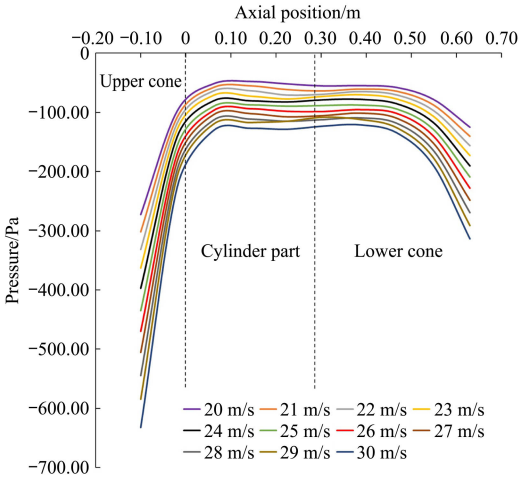

e. Effects of the MOG outlet air velocity on the negative pressure along the center axis

Figure 7 Effects of the MOG outlet air velocity on the airflow status

obvious influence on them. In plane 2, the average air velocity was not higher than the air velocity of the high-velocity area when the outlet air velocity was higher than 27 m/s due to the quick increase of the air velocity in the low-velocity area. Similarly, the increasing rate slowed down because of the stability of the axial air velocity in the low-velocity area when the outlet air velocity was higher than 23 m/s. In terms of the axial air velocity distribution along the center axial, the air velocity in the cylinder part was higher while the velocity in the lower cone was the lowest when the outlet air velocity was 20 m/s. The increasing rate of the air velocity in the cylinder part was higher when the outlet air velocity was 29 m/s. In terms of the axial pressure distribution along the center axial, the negative pressure increased with the increase of the outlet air velocity.

3.3 Optimal parameters combination

In this research, the response surface experiment was carried out to find out the optimal combination of the inlet and outlet velocities. The range of the inlet air velocity and the outlet air velocity was 1-5 m/s and 20-30 m/s, respectively, the same as that in the single factor experiments. Table 1 lists the factors and levels of the experiment. The results were listed in Table 2.

The relationship between the actual factors and indexes could be obtained as follows:

$$y_1 = -3.94 + 0.073x_1 + 0.46x_2 - 0.021x_1x_2 + 0.028x_1^2 - 0.0021x_2^2 \quad (3)$$

$$y_2 = -6.13 + 0.12x_1 + 0.65x_2 - 0.013x_1x_2 - 0.014x_1^2 - 0.0063x_2^2 \quad (4)$$

$$y_3 = 1.17 - 0.044x_1 - 0.074x_2 - 0.013x_1x_2 + 0.048x_1^2 + 0.0036x_2^2 \quad (5)$$

$$y_4 = 0.74 - 0.81x_1 + 0.22x_2 + 0.027x_1x_2 - 0.021x_1^2 - 0.0022x_2^2 \quad (6)$$

$$y_5 = 1.41 - 0.83x_1 + 0.2x_2 + 0.023x_1x_2 + 0.011x_1^2 - 0.0024x_2^2 \quad (7)$$

$$y_6 = -0.078 - 0.2x_1 + 0.046x_2 + 0.01x_1x_2 - 0.033x_1^2 + 0.00025x_2^2 \quad (8)$$

The p values of the above regression models were all less than 0.01, indicating that the models can correctly reflect the relationship between the working parameters and the air velocity at the key positions in the cyclone separator.

Table 1 Factors and levels of the response surface experiment

Factors	Levels				
	–1.414	–1	0	1	1.414
Inlet air velocity (x_1)/m·s^{-1}	1	1.6	3	4.4	5
Outlet air velocity (x_2)/m·s^{-1}	20	21.5	25	28.5	30

Table 2 Results of the response surface experiment

No.	Inlet air velocity (x_1)/m·s^{-1}	Outlet air velocity (x_2) /m·s^{-1}	Average air velocity in plane 1 (y_1) /m·s^{-1}	High-velocity in plane 1 (y_2) /m·s^{-1}	Low-velocity in plane 1 (y_3) /m·s^{-1}	Average air velocity in plane 2 (y_4) /m·s^{-1}	High-velocity in plane 2 (y_5) /m·s^{-1}	Low-velocity in plane 2 (y_6) /m·s^{-1}
1	4.4	28.5	5.48	5.88	1.03	4.70	4.80	1.18
2	3.0	25.0	5.04	5.47	0.89	4.27	4.34	1.08
3	3.0	25.0	5.04	5.47	0.89	4.27	4.34	1.08
4	3.0	20.0	3.38	3.70	0.57	3.27	3.61	0.57
5	3.0	25.0	5.04	5.47	0.89	4.27	4.34	1.08
6	3.0	25.0	5.04	5.47	0.89	4.27	4.34	1.08
7	4.4	21.5	3.87	4.07	0.81	3.04	3.36	0.53
8	3.0	25.0	5.04	5.47	0.89	4.27	4.34	1.08
9	1.6	21.5	4.50	4.77	0.91	4.03	4.12	1.00
10	1.6	28.5	6.53	6.84	1.38	5.17	5.11	1.45
11	5.0	25.0	4.56	4.80	0.95	3.60	4.00	0.60
12	3.0	30.0	6.55	6.88	1.38	5.10	4.92	1.56
13	1.0	25.0	5.70	5.98	1.21	4.71	4.74	1.25

According to the response surface curve of interaction factors on the airflow distribution of plane 1 (Figure 8), when the inlet air velocity was at zero level (3 m/s), the average velocity, the velocity of the high-velocity area, and the velocity of the low-velocity airflow area all increased with the increase of the MOG outlet air velocity. When the MOG outlet air velocity was at zero level (25 m/s), the average velocity and the velocity of the high-velocity area both decreased with the increase of the inlet air velocity, and the velocity of the low-velocity area first decreased and then increased. The reason was that the two airflows collided in the low-velocity area to form a slight disturbance. The response surface curve changed faster along the x_1 direction, indicating that the MOG outlet air velocity had more influence on the airflow field distribution than the inlet air velocity.

According to the response surface curve of interaction factors on the airflow distribution of plane 2 (Figure 9), when the inlet air velocity was at zero level (3 m/s), the average velocity, the velocity of the high-velocity area, and the velocity of the low-velocity airflow area all increased with the increase of the MOG outlet air velocity. When the MOG outlet air velocity was at zero level (25 m/s), all the velocities decreased with the increase of the inlet air velocity. There was little difference in the changes of the response surface curve along the x_1 and x_2 directions, indicating that the MOG outlet air velocity and the inlet air velocity both had significant influence on the airflow field distribution in plane 2.

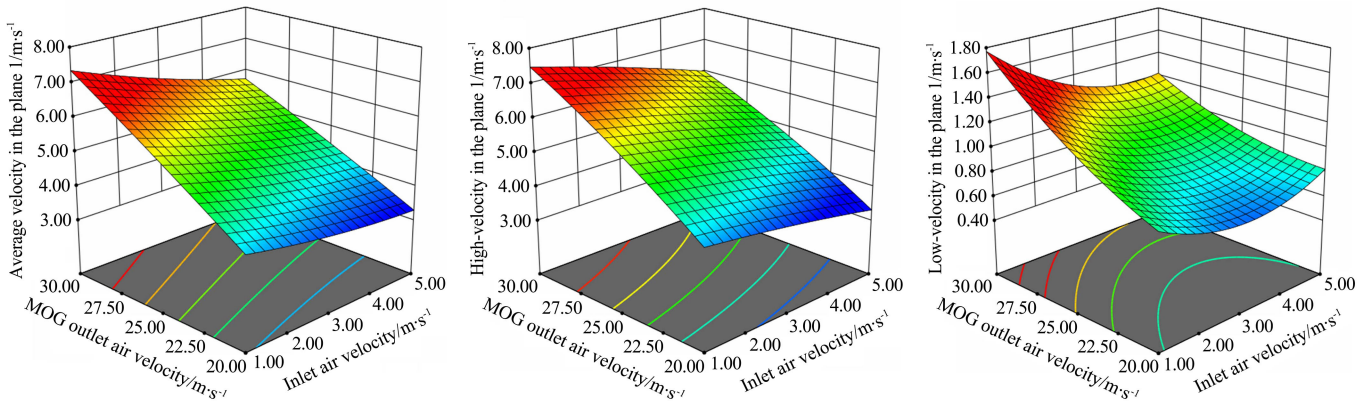

a.Influence of MOG outlet air velocity and inlet air velocity on average velocity in plane 1

b. Influence of MOG outlet air velocity and inlet air velocity on high-velocity in plane 1

c. Influence of MOG outlet air velocity and inlet air velocity on low-velocity in plane 1

Figure 8 Response surfaces of airflow velocities in plane 1 to interactive factors

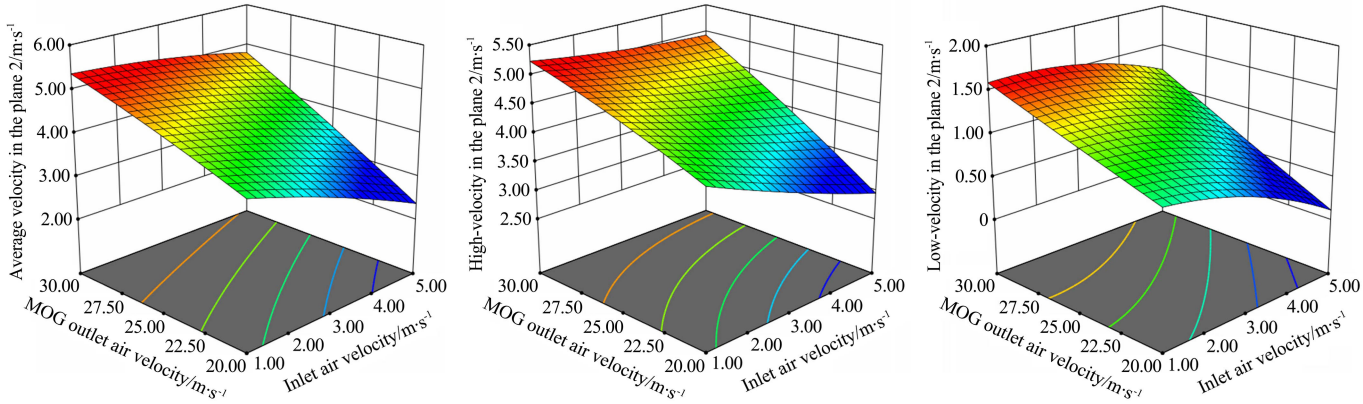

a. Influence of MOG outlet air velocity and inlet air velocity on average velocity in plane 2

b. Influence of MOG outlet air velocity and inlet air velocity on high-velocity in plane 2

c. Influence of MOG outlet air velocity and inlet air velocity on low-velocity in plane 2

Figure 9 Response surfaces of airflow velocities in plane 2 to interactive factors

The difference between the velocities of the high-velocity and the low-velocity areas could be utilized to represent the performance of the high-velocity area. The larger the difference meant the high velocity was more concentrated. At the same time, the average air velocities of horizontal planes should be close to ensure the stability of the airflow in the cylinder part. As a result, the targets and constraints of the optimization were as below.

The targets were:

$$\begin{cases} \max_{(y_2,y_3)} = y_2 - y_3 \\ \max_{(y_5,y_6)} = y_5 - y_6 \\ \min_{(y_1,y_4)} = y_1 - y_4 \end{cases} \tag{9}$$

The constraints were:

$$\begin{cases} y_2 \geq 6.3 \\ y_3 \geq 1.2 \end{cases} \tag{10}$$

The optimal combination of the inlet air velocity and MOG outlet air velocity was 4.25 m/s and 29.87 m/s, respectively. To validate the results, a simulation under this condition was carried out. The comparison of the data from the calculation and the simulation are listed in Table 3. It showed that these values obtained by calculation and simulation were basically consistent. The equations that represented the relationship between the working parameters and indexes could be used to predict the performance of the cyclone in a certain range.

Table 3 Validation of the optimal parameters combination

Values	y_1/m·s^{-1}	y_2/m·s^{-1}	y_3/m·s^{-1}	y_4/m·s^{-1}	y_5/m·s^{-1}	y_6/m·s^{-1}
Calculation	6.07	6.27	1.20	4.96	4.84	1.34
Simulation	5.97	6.33	1.18	4.98	4.97	1.37

In addition, the airflow field distribution in the cyclone separator under the optimal combination of working parameters is shown in Figure 10. Although the airflows from inlet and MOG outlet had certain disturbances, the high-velocity area was still relatively symmetrical. The corresponding thrower rate and fan rate in the bench test were 278 r/min and 1972 r/min, respectively. And, the average cleaning ratio and loss ratio were 96.14% and 6.09%, respectively.

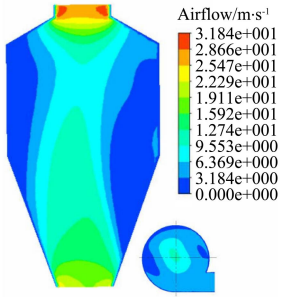

Figure 10 Airflow status under optimal working parameter combination

3.4 Field validation

The field experiments were carried out at the experimental fields of Huazhong Agricultural University, as shown in Figure 11. The planting density was 38 plants/m^2, the average plant height was 1757 mm, and the moisture content of the main stem, pod, and rapeseed were 58.04%, 36.83%, and 24.55%, respectively. The air velocities of the inlet and MOG outlet were controlled by adjusting the speed of the blower and fan during the field validation. The inlet air velocity and MOG outlet air velocity were set as 4.3 m/s and 29.9 m/s, respectively.

The forward speed of the harvester was adjusted based on the status of the rapeseed plant and field conditions to keep the feed rate in the range of 2.0-3.0 kg/s. The cyclone separation cleaning device could work well. The cleaning ratio and loss ratio were 94.62% and 5.39%, respectively. It showed that cyclone separator could meet the needs of rapeseed cleaning.

Figure 11 Field experiment carried out for this study

4 Conclusions

In this research, the influence of the inlet and the MOG outlet air velocities on the high-velocity and low-velocity areas inside the cyclone separator was gained by the CFD approach. Furthermore, a prediction model built by the response surface experiment was utilized.

1) The difference between the velocities of the high-velocity and the low-velocity areas could be utilized to represent the performance of the high-velocity area. The larger the difference meant the high velocity was more concentrated. At the same time, the average air velocities of horizontal planes should be close to ensure the stability of the airflow in the cylinder part.

2）The mathematical model of the relationship between the air velocities inside the cyclone and the working parameters was built. The better combination of the inlet and MOG outlet velocities were 4.25 m/s and 29.87 m/s, respectively. The calculated velocities were basically the same as the results obtained by the validated simulation.

3) Under the optimal combination of working parameters, the cyclone separation cleaning device could work well. In the field, the cleaning ratio and loss ratio were 94.62% and 5.39%, respectively. The cyclone separator could meet the needs of rapeseed cleaning.

The airflow field distribution in the cyclone separator is not only related to the working parameters but also related to the structural parameters. In the future, the cyclone separation cleaning device will be further optimized based on the influence of the structural parameters on the airflow field, and the gas-solid coupling mechanism will be explored by CFD-EDEM coupling method.

Acknowledgements

This research was financially supported by the National Natural Science Foundation of China (Grant No. 52205270 and No. 52075210), the China Postdoctoral Science Foundation (Grant No. 2020M682438), and China Agriculture Research System of MOF and MARA (Grant No. CARS-12).

[References]

[1] Jiang T, Zhang M, Guan Z H, Mu S L, Wu C Y, Wang G, et al. Simulation and analysis of the pneumatic recovery for side-cutting loss of combine harvesters with CFD-DEM coupling approach. Int J Agric & Biol Eng, 2022; 15(2): 117–126.

[2] Hobson R N, Bruce D M. Seed loss when cutting a standing crop of oilseed rape with two types of combine harvester header. Biosystems Engineering, 2002; 81(3): 281–286.

[3] Wu C Y, Xiao S Y, Jin M. Comparation on rape combine harvesting and two-stage harvesting. Transactions of the CSAE, 2014; 30(17): 10–16. (in Chinese)

[4] Szpryngiel M, Wesołowski M, Szot B. Economical technology of rape seed harvest. Teka Komisji Motoryzacji IEnergetyki Rolnictwa, 2003; 4(1): 185–195.

[5] Ma N, Zhang C L, Li J, Zhang M H, Cheng Y G, Li G M, et al. Mechanical harvesting effects on seed yield loss, quality traits and profitability of winter oilseed rape (*Brassicanapus* L.). Journal of Integrative Agriculture, 2012; 11(8): 1297–1304.

[6] Li H T, Liao Q X, Li P, Huang P, Wan X Y, Ji M Y. Design on separating-combined header of rape combine harvester. Journal of Huazhong Agricultural University, 2014; 33(5): 111–116. (in Chinese)

[7] Craessaerts G, Saeys W, Missotten B, De Baerdemaeker J. Identification of the cleaning process on combine harvesters. Part I: A fuzzy model for prediction of the material other than grain (MOG) content in the grain bin. Biosystems Engineering, 2008; 101(1): 42–49.

[8] Dai F, Song X F, Shi R J, Guo W J, Zhao Y M, Wang F, et al. Movement law of the threshing material in threshing and cleaning machine for plot-bred wheat. Int J Agric & Biol Eng, 2022; 15(3): 100–106.

[9] Chen L, Liao Q X, Zong W Y, Liao Y T, Li H T, Huang P. Aerodynamic characteristics measurement of extraction components for rape combine harvester. Transactions of the CSAM, 2012; 43(S1): 125–130. (in Chinese)

[10] Ni C A, Zhang L J, Liu S D, Shi Q X, Gao C Y, Geng L X. Experimental analysis on cyclone separating cleaning system of no-guide vanes. Transactions of the CSAE, 2008; 24(8): 135–138. (in Chinese)

[11] Liao Q X, Wan X Y, Li H T, Ji M Y, Wang H. Design and experiment on cyclone separating cleaning system for rape combine harvester. Transactions of the CSAE, 2015; 31(14): 24–31. (in Chinese)

[12] Wan X Y, Shu C X, Xu Y, Yuan J C, Li H T, Liao Q X. Design and experiment on cylinder sieve with different rotational speed in cleaning system for rape combine harvesters. Transactions of the CSAE, 2018; 34(14): 27–35. (in Chinese)

[13] Wan X Y, Liao Q X, Yang X, Yuan J C, Li H T. Design and evaluation of cyclone separation cleaning devices using a conical sieve for rape combine harvesters. Applied Engineering in Agriculture, 2018; 34(4): 677–686.

[14] Jin X, Du X W, Gan B X, Ji J T, Dong X, Wang G X. Cleaning performance experiment of cyclone separating sys-tem in miniature combine harvester. Transactions of the CSAM, 2016; 47(5): 99–105. (in Chinese)

[15] Azadi M, Azadi M, Mohebbi A. A CFD study of the effect of cyclone size on its performance parameters. Journal of Hazardous Materials, 2010; 182(1-3): 835–841.

[16] Mazyan W I, Ahmadi A, Ahmed H, Hoorfar M. Enhancement of solid particle separation efficiency in gas cyclones using electro-hydrodynamic method. Separation and Purification Technology, 2017; 182: 29–35.

[17] Dong Y P, Dong L, Qiang N, Jing Y Z, Guo F Q. Numerical simulation of biomass gas and tar torrential flow characteristics in cyclone separator. Transactions of the CSAE, 2010; 26(9): 171–175. (in Chinese)

[18] Elsayed K, Lacor C. Optimization of the cyclone separator geometry for minimum pressure drop using mathematical models and CFD simulations. Chemical Engineering Science, 2010; 65(22): 6048–6058.

[19] Hamed S, Javid Z, Mohammadreza M. Numerical study of flow field in new design cyclone separators with one, two and three tangential inlets. Advanced Powder Technology, 2018; 29(3): 611–622.

[20] Huang Y, Zhao M Q. Optimization design of performance test of cyclone separator sand sampler based on numerical simulation and wind erosion tunnel experiment. Transactions of the CSAE, 2015; 31(16): 50–56. (in Chinese)

[21] Zhao X G, Xu L M, Gao L X, Li X Q. Simulation of soybean thresher cyclone separating and cleaning system. Transactions of the CSAM, 2014; 45(S1): 80–87. (in Chinese)

[22] Wan X Y, Liao Y T, Yuan J C, Yang J, Liao Q X. Numerical analysis of cyclone separator with different structural parameters for rapeseed combine harvester based on CFD. 2021 ASABE Annual International Virtual Meeting, 2021; pp.533–546. doi: 10.13031/aim.202100160.